Two-pulse photon echo area theorem in an optically dense medium

R. Urmancheev, K. Gerasimov, M. Minnegaliev, T. Chanelière, A. Louchet-Chauvet, S. S Moiseev

Research Article | Vol. 27, No. 20 | 30 Sep 2019 | OPTICS EXPRESS 28983
Optics EXPRESS

Two-pulse photon echo area theorem in an optically dense medium

R. URMANCHEEV,[1] K. GERASIMOV,[1] M. MINNEGALIEV,[1] T. CHANELIÈRE,[2] A. LOUCHET-CHAUVET,[2] AND S. MOISEEV[1,*]

[1]*Kazan Quantum Center, Kazan National Research Technical University n.a. A.N.Tupolev-KAI, 10 K. Marx, Kazan 420111, Russia*
[2]*Laboratoire Aimé Cotton, CNRS, Univ. Paris-Sud, ENS Cachan, Université Paris-Saclay, 91405 Orsay Cedex, France*
[*]*samoi@yandex.ru*

Abstract: We perform a theoretical and experimental study of the two-pulse photon echo area conservation law in an optically dense medium. The experimental properties of the echo signal are studied at 4K on the optical transition $^3H_6(1)\rightarrow{}^3H_4(1)$ (793 nm) of Tm^{3+} in a YAG crystal for a wide range of pulse areas of the two incoming light pulses, up to $\theta_1 \approx 4\pi$ and $\theta_2 \approx 7\pi$ respectively, with optical depth 1.5. We analyze the experimental data by using the analytic solution of the photon echo area theorem for plane waves. We find that the transverse Gaussian spatial profile of the beam leads to an attenuation of the echo area nutation as function of θ_1 and θ_2. Additional spatial filtering of the photon echo beam allows to recover this nutation. The experimental data are in good agreement with the solution of photon echo pulse area theorem for weak incoming pulse areas $\theta_{1,2} \lesssim \pi$. However at higher pulse areas, the observations diverge from the analytic solution requiring further theoretical and experimental studies.

1. Introduction

The optical analogue of the spin echo [1], the photon echo [2,3] is an efficient method in modern coherent spectroscopy [4]. It became a well-established tool to extract basic spectroscopic parameters of optical transitions and characterize fast atomic and molecular quantum dynamics up to the femtosecond timescale [5–10]. In applied research, the photon echo has been considered in the 70's as a tool for the fast storage and processing of the optical information [11–16]. More recently, it has been shown that modified schemes of photon echo in optically dense media can be efficiently applied for the quantum storage of photonic qubits [17–23], even if the use of strong π-pulses could be risky [24,25]. We take a widely used definition of optical density: the absorption coefficient multiplied by the sample thickness.

In this broad context, the McCall-Hahn pulse area theorem provides a global description of light pulse propagation in optically dense resonant atomic media [26]. The theorem can be seen as a general conservation law for the pulse area and a helpful complement to the energy conservation law. In essence, the area law is independent of the particular temporal shapes of the input pulses and is widely used as a descriptive parameter for spin and photon echo measurements. After 50 years, the theorem continues to attract researchers' attention [27–34]. Experimental studies of the pulse amplitude, spatial beam profile, temporal pulse shape and medium optical thickness on the photon echo intensity are usually described by the Maxwell-Bloch numerical simulation [35–39] or by using area theorem for a small input pulse area [40,41]. The most general case of the photon echo area theorem, *i.e.* valid for any arbitrary incoming pulse intensities, was also discussed in [42,43] in terms of total pulse area of all the generated signals. The analytical solution of the photon echo pulse area was obtained in [44] for arbitrary areas of the incoming pulses. Below we analyze these solutions and compare with new experimental results and existing numerical calculations [36].

#356012 https://doi.org/10.1364/OE.27.028983
Journal © 2019 Received 21 Dec 2018; revised 13 Mar 2019; accepted 14 Mar 2019; published 25 Sep 2019

Optics EXPRESS

It is worth noting that in the recent context of quantum information with the realization of optical quantum memories, the photon echo area theorem could provide general understanding of the signal propagation in optically dense samples [17, 18, 20, 45]. The small input pulse area condition is not only a particular case of the area theorem but also a limitation for the quantum storage fidelity [24, 25]. In any case, the recent progress in the extreme field confinement achieved for rare-earth ions embedded in photonic cavities should revive the interest in the area theorem since large areas can be obtained with only a few photons when the so-called strong confinement regime is targeted [46–48].

In the second section, we give a theoretical description of the photon echo pulse area theorem in an optically dense medium. In the next section, we present the experimental results obtained for a two-pulse photon echo sequence in a Tm^{3+}:YAG crystal (c = 0.1 at. %). We vary the input pulse areas up to $\theta_1(0) \approx 4\pi$ and $\theta_2(0) \approx 7\pi$ for the first and second pulses respectively. The obtained experimental data are discussed in the light of the analytical solution for the photon echo area theorem, including the transverse Gaussian profile of the light beam. We partially retrieve the plane wave solution by using spatial filtering of the light beams.

2. Photon echo area theorem

We derive in this section the area theorem for the echo in a two-pulse photon echo sequence depicted in Fig. 1. We first remind the well-known McCall-Hahn area theorem for a single pulse.

2.1. Pulse area theorems: plane wave solutions

2.1.1. McCall-Hahn area theorem

Following [26, 27, 44] and using the well-established Bloch-Maxwell formalism in one dimension (propagation along z) for two-level inhomogeneously broadened atomic ensemble, the pulse area $\theta_1(z)$ follows the propagation equation known as the McCall-Hahn area theorem [26]:

$$\frac{\partial\theta_1(z)}{\partial z} = -\frac{1}{2}\alpha \sin\theta_1(z), \tag{1}$$

where α is the resonant absorption coefficient [42]. The solution of this equation is:

$$\theta_1(z) = 2\arctan\left[e^{-\alpha z/2}\tan\frac{\theta_1(0)}{2}\right]. \tag{2}$$

An important consequence of Eq. (2) is that if the incident pulse has a pulse area $\theta_1(0) = k\pi$, $k \in \mathbb{Z}$, then the area is conserved during the propagation. This is true for even values of k as noted in the original work [26] as well as for odd values of k. However, the latter case is much more difficult to implement experimentally, since the initial pulse area is preserved only when $\theta_1(0)$ is very close or exactly equal to π, otherwise the pulse area converges towards the nearest even multiple of π while propagating.

2.1.2. Photon echo area theorem

Following the same approach, the theorem was extended to a two-pulse photon echo sequence. The pulse areas of second input pulse and photon echo follow the equations derived in [27] and [44]:

$$\frac{\partial\theta_2(z)}{\partial z} = -\frac{1}{2}\alpha \cos\theta_1(z)\sin\theta_2(z), \tag{3}$$

$$\frac{\partial\theta_e(z)}{\partial z} = \frac{1}{2}\alpha\left[2e^{-2\tau_{12}/T_2}\sin\theta_1(z)\sin^2\frac{\theta_2(z)}{2}\cos^2\frac{\theta_e(z)}{2} - \cos\theta_1(z)\cos\theta_2(z)\sin\theta_e(z)\right], \tag{4}$$

Optics EXPRESS

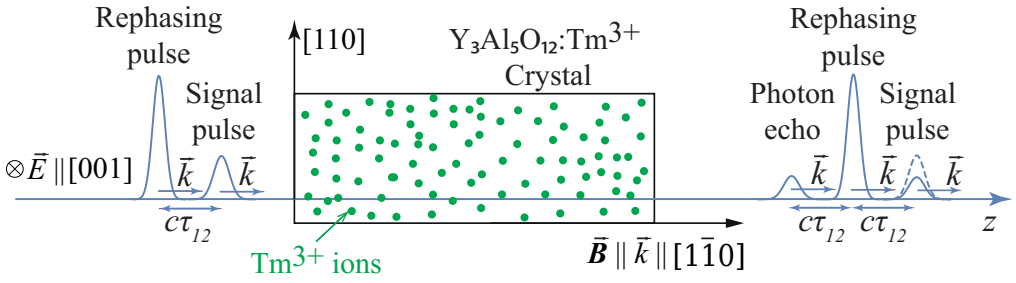

Fig. 1. The classic two pulse echo sequence propagation through the Tm^{3+} doped crystal. $\vec{k}$ is the common wave vector of three pulses parallel to the external magnetic field. The first signal pulse is partly absorbed by the medium, the second pulse triggers the rephasing process which results in the photon echo emission.

where $\theta_i(z), i = 1, 2, e$ are the pulse areas of the first, second and echo pulses respectively, τ_{12} is the delay between the incoming pulses, and T_2 is the coherence lifetime of the atomic transition. A detailed derivation of Eqs. (3) and (4) can be found in the Appendix.

Equations (1) and (3) describe the area propagation of first two pulses (see also [42]). In turn, Eq. (4) characterizes the echo generated at $t = 2\tau_{12}$ when it is well separated temporally from the first two pulses $\tau_{12} \gg \delta t_{1,2}$ (see Appendix for details). The analytical solution of Eqs. (3) and (4) given in [44] can be rewritten in the form :

$$\theta_2(z) = 2\arctan\left[\gamma\,\mathrm{sech}\left(\beta - \frac{\alpha}{2}z\right)\right], \tag{5}$$

$$\theta_e(z) = 2\arctan\left[e^{-2\tau_{12}/T_2}\sin\theta_1(0)\sin^2\frac{\theta_2(z)}{2}\sinh\frac{\alpha z}{2}\right], \tag{6}$$

where $\sin^2\frac{\theta_2(z)}{2} = \dfrac{\gamma^2}{[\cosh^2(\beta - \frac{\alpha}{2}z) + \gamma^2]}$ with $\beta = \ln\{\tan[\frac{\theta_1(0)}{2}]\}$ and $\gamma = \tan[\frac{\theta_2(0)}{2}]/\sin[\theta_1(0)]$ for $\theta_1(0) < \pi$. For other values $\theta_1(0) > \pi$ one can use a more explicit formula: $\sin^2\dfrac{\theta_2(z)}{2} = \gamma^2/\left[\left(\tan\dfrac{\theta_1(0)}{2}e^{-\frac{\alpha}{2}z} + \cot\dfrac{\theta_1(0)}{2}e^{\frac{\alpha}{2}z}\right)^2 + \gamma^2\right]$.

According to the solution (5) (see also [43]), at the particular case $\theta_2(0) = \pi$ second pulse area remains unchanged during propagation independently of the first pulse area i.e. $\theta_2(z) = \pi$.

The solution for the echo pulse area (6) is in agreement with the direct Maxwell-Bloch numerical simulations given in [36]. In particular the authors considered two cases: $\theta_2(0) = \pi$ and $\theta_2(0) = \pi/2$ ($T_2 \gg \tau_{12}$, $\theta_1(0) = 0.27\theta_2(0), \delta t_1 > \delta t_2$) and calculated the pulse energy efficiency as a function of optical depth αL. The calculated energy efficiency behavior coincides with the $\theta_e^2(z)/\theta_1^2(0)$ dependence depicted in Fig. 2. This agreement clearly shows the potential of the area theorem approach to quantitatively characterize the nonlinear interaction in optically dense media.

Let us now discuss the basic properties of the photon echo pulse area theorem in few particular cases.

First pulse area is a multiple of π. Here we have two limiting cases are:

1. $\theta_1(0) \to (2n+1)\pi$, where $\sin^2\dfrac{\theta_2(z)}{2} \to \dfrac{\tan^2[\frac{\theta_2(0)}{2}]}{e^{-\alpha z} + \tan^2[\frac{\theta_2(0)}{2}]}$ and $\lim_{\alpha z\to\infty}\theta_2(z) = (2n+1)\pi$,

Optics EXPRESS

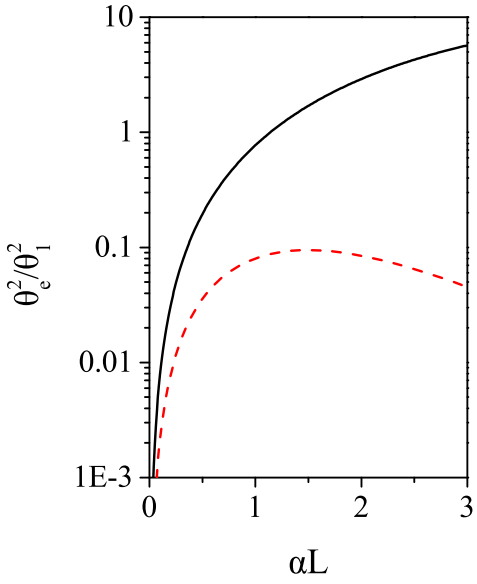

Fig. 2. An area counterpart of the Fig. 2 of [36], plotting the energy efficiency of the echo pulse $\theta_e^2/\theta_1^2(0)$ without relaxation, i.e. $T_2 = \infty$. The incoming pulses' areas are $\theta_1(0) = 0.27\pi, \theta_2(0) = \pi$ for the solid black curve and $\theta_1(0) = 0.27\pi/2, \theta_2(0) = \pi/2$ for the red dashed curve.

2. $\theta_1(0) \to 2m\pi$, where $\sin^2\dfrac{\theta_2(z)}{2} \to \dfrac{\tan^2[\frac{\theta_2(0)}{2}]}{e^{\alpha z} + \tan^2[\frac{\theta_2(0)}{2}]}$ and $\lim_{\alpha z\to\infty}\theta_2(z) = 2\pi m$,

where $n, m = 0, 1, 2, \ldots$.

These two cases satisfy the condition $\lim_{\alpha z\to\infty}\{\theta_1(z) + \theta_2(z)\} = 2\pi(n+m)$, demonstrating an asymptotic formation of optical solitons after interacting with the second pulse. This situation actually corresponds to the McCall-Hahn theorem [26,42] due to the absence of photon echo in these cases (due to re-absorption).

Echo in an optically thin medium When $\alpha z \ll 1$, Eq. (6) simplifies as:

$$\theta_e(z) = e^{-2\tau_{12}/T_2}\alpha z \cdot \sin\theta_1(0)\sin^2\frac{\theta_2(0)}{2}. \tag{7}$$

This solution was studied earlier in [3,41,49].

Standard photon echo ($\pi/2$,π)-excitation This is the most popular case of the photon/spin echo spectroscopy with $\theta_1(0) = \pi/2$, $\theta_2(0) = \pi$ (which gives $\beta = 0$, $\gamma = \infty$ in Eq. (6), and $\theta_2(z) = \pi$) so we can obtain the simplified solution:

$$\theta_e(z) = 2\arctan\left[e^{-2\tau_{12}/T_2}\sinh\frac{\alpha z}{2}\right]. \tag{8}$$

The echo pulse area is continuously amplified in the medium by the factor $\sinh(\frac{\alpha z}{2})$ with the asymptotic values for the gain: $\sinh\frac{\alpha z}{2} \to \frac{1}{2}\exp\frac{\alpha z}{2}$ and the echo area $\theta_e(z) \to \pi$ in the limit $\alpha z \to +\infty$. In this limit, the total area of the three pulses $\theta_1(z) + \theta_2(z) + \theta_e(z) \to 2\pi$, when the first pulse is completely absorbed and the area of the second pulse remains π. This also ensures the absence of any secondary echo pulse.

Optics EXPRESS

Weak first pulse ($\theta_1(0) \ll \pi$) This case typically corresponds to quantum memory schemes based on the photon echo in ensembles [19,50]. Assuming $\theta_1(0) \ll \pi$, Eq. (6) leads to:

$$\theta_e(z) = 2\arctan\left[e^{-2\tau_{12}/T_2}\theta_1(0)\sin^2\frac{\theta_2(z)}{2}\sinh\frac{\alpha z}{2}\right], \tag{9}$$

An intense echo can also be retrieved when $\theta_2(0) = \pi$ despite the small incoming pulse area. In that case, we obtain from Eq. (9):

$$\theta_e(z) = 2\arctan\left[e^{-2\tau_{12}/T_2}\theta_1(0)\sinh\frac{\alpha z}{2}\right]. \tag{10}$$

This expression shows that the echo pulse tends to a π-pulse in a sufficiently large optical depth. Area and energy efficiencies can be greater than unity [36,43,51]. This comes from pulse echo amplification in an inverted medium and leads to quantum noise when the photon echo is considered as a memory [25].

We see that initial condition $\theta_1(0) \ll 1$ does not guarantee that the small echo pulse area $\theta_e(z) \ll 1$ condition is maintained though propagation because of the echo amplification by the gain term $\sinh\frac{\alpha z}{2}$. Equation (9) gives the appropriate condition for the weak first pulse approximation $\theta_1(0) < 1/\left(\sin^2\frac{\theta_2(z)}{2}\sinh\frac{\alpha z}{2}\right)$ at any position $z \le L$. In the special case $\theta_2(0) = \pi$ and $\tau_{12} \ll T_2$, this translates into the condition $\theta_1(0) < 1/\left(\sinh\frac{\alpha L}{2}\right) \approx 2e^{-\alpha L/2}$ leading to the solution of Eq. (9) [25]:

$$\theta_e(z) = 2e^{-2\tau_{12}/T_2}\theta_1(0)\sin^2\frac{\theta_2(z)}{2}\sinh\frac{\alpha z}{2}. \tag{11}$$

Non-optimal photon echo generation ($\theta_2(0) \neq \pi$) The echo pulse amplification can be suppressed by the spatially dependent factor $\sin^2(\theta_2(z)/2)$ for $z > 2\beta/\alpha$ if the input pulse area of the second light pulse $\theta_2(0) \neq \pi$. For sufficiently large input pulse area of the first pulse $\theta_1(0) > 1$ in Eq. (6) and $\theta_2(0) \neq \pi$, we have the following asymptotic decrease of the echo pulse area:

$$\theta_e(z) = 2\arctan\left[e^{-2\tau_{12}/T_2}\sin\theta_1(0)\frac{\gamma^2\sinh\frac{\alpha z}{2}}{[\gamma^2+\cosh^2(\beta-\frac{\alpha z}{2})]}\right]_{\alpha z\gg 1} \cong$$
$$2\arctan\left[2\exp\left(-2\tau_{12}/T_2+2\beta\right)\frac{\tan^2[\frac{\theta_2(0)}{2}]}{\sin[\theta_1(0)]}\exp\left(-\frac{\alpha z}{2}\right)\right]. \tag{12}$$

Equation (12) shows that echo signal is generated and propagates only at the entrance of the atomic medium. We also find in Eq. (12) that an optical soliton is formed at $z/\alpha \gg 1$ [26,42] if $\theta_2(0) > \pi$. A wide range of interesting physical effects associated with the soliton formation is however beyond the scope of this paper. Equation (12) shows that in optically dense media, the echo pulse area can take any values in the interval $[-\pi,\pi]$ starting from zero, it peaks at some value of z and then decays to zero with $z \to \infty$. The fact that area of each echo pulse is less than π does not contradict with the McCall-Hahn area theorem [26,40] predicting 2π pulse formation, when $\theta_1(0) + \theta_2(0) > \pi$. It only means that one needs to consider also higher order echos (after the primary echo) which are also exciting the medium.

In summary, Fig. 3 shows the photon echo pulse area as a function of the second incoming pulse area $\theta_2(0)$ for different optical depths of the medium αL. We examine the previously

Optics EXPRESS

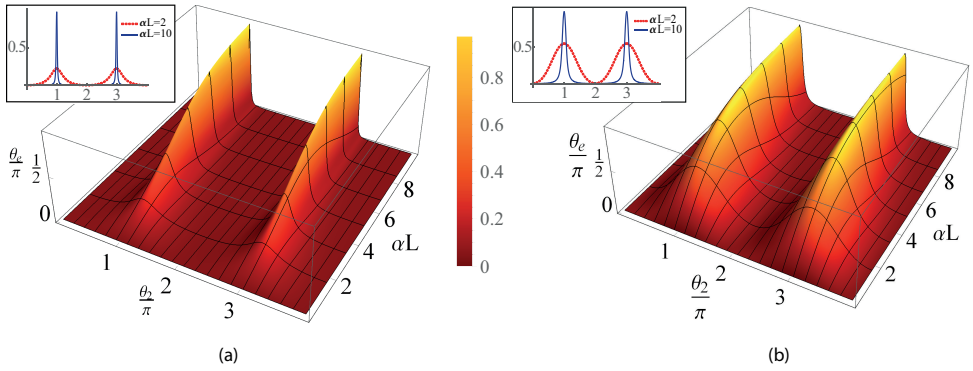

Fig. 3. 3D plot of the photon echo area theorem solution Eq. (6) $\theta_e(\theta_2(0), \alpha L)$ for (a) $\theta_1(0) = 0.1\pi$ (weak first pulse case) and (b) $\theta_1(0) = \pi/2$ as function of the incoming second pulse area $\theta_2(0)$ (in the units of π) and optical density αL of the medium. The insets in (a) and (b) show the cross sections at $\alpha L = 2$ (red dashed curve) and $\alpha L = 10$ (blue solid curve).

discussed cases: $\theta_1(0) \ll \pi$ with $\theta_1(0) = 0.1\pi$ in Fig. 3(a) and $\theta_1(0) = \pi/2$ in Fig. 3(b). For a given optical density αL, the photon echo pulse area $\theta_e(\theta_2(0))$ undergoes a series of oscillations peaking at $\theta_2(0) = (2n + 1)\pi$. It is interesting to note that the positions of the maxima are independent of $\theta_1(0)$. The peak widths, however, become sharper at higher optical densities. The insets in Figs. 3(a) and 3(b) show the cross sections at $\alpha L = 2$ and $\alpha L = 10$ and reveal these tendencies. The non-linear nature of the process in an optically dense ($\alpha L \gg 1$) medium causes the echo to form practically only when the second incoming pulse area is an odd multiple of π. For $\theta_2(0) \neq (2n + 1)\pi$, the echo area is maximum at a specific optical depth and then decreases with the increase of αL. On the contrary, for $\theta_2(0) = \pi$ the echo area asymptotically tends towards π which could lead to area efficiency $|\theta_e(L)/\theta_1(0)|^2 > 1$ only limited by finite optical density αL, relaxation time T_2 and non-ideality of π-pulse.

Below we experimentally test the photon echo area theorem in more general conditions, namely high incoming pulse areas $\theta_1(0) > \pi, \theta_2(0) > 2\pi$ and different spatial filtering profiles.

2.2. *Including the transverse Gaussian beam profile*

In our experiments, the light beams have a Gaussian profile so the field in the atomic medium is described by $E(t, r) = E_0(t)e^{-(r/r_0)^2}$ where r is the transverse coordinate and r_0 the beam radius. A complete study of the Maxwell-Bloch equations in two dimensions z and r is a complex problem well beyond the scope of this work. Indeed, the two-level dynamics induces additional highly non-linear terms in the field master equation (paraxial Helmholtz equation with a source term). We extend in a simple manner the photon echo area Eqs. (1), (3) and (6) derived for plane waves to include the transverse spatial beam profile and give a quantitative explanation of the experimental data. For the sake of simplicity, we assume the geometrical optics approximation *i.e.* neglect diffraction effects (similar to the studies of the resonators stability presented by Siegman in [52]). This assumption is valid for a sufficiently large beam cross-section $\pi r_0^2 \gg L\lambda$ (λ is the wavelength of light). However, it should be noted that in our experimental conditions, the inequality is not fulfilled ($\pi r_0^2 = 0.3L\lambda$) to favour large pulse areas. So diffraction effects could play a considerable role in our case.

We include the transverse spatial coordinates r of the incoming pulses in the photon echo areas

Optics EXPRESS

$\theta_{1,2,e}(r,z)$. Assuming that the input pulse areas $\theta_1(r,0)$, $\theta_2(r,0)$ have Gaussian spatial profiles at the entrance of the atomic medium $z = 0$, we obtain for the echo pulse area Eq. (6) in the geometrical optics limit:

$$\theta_e(r,z) = 2\arctan\left[e^{-2\tau_{12}/T_2}\sin\theta_1(r,0)\sin^2\frac{\theta_2(r,z)}{2}\sinh\frac{\alpha z}{2}\right]. \tag{13}$$

Experimentally, the medium is imaged onto a detector with a magnification factor M. The measured detector signal is proportional to the field intensity averaged over the active detection surface. This latter can be connected to the theoretically calculated $\theta_e(r,L)$ (see Eq. (13)) by

$$\langle\theta_e^2(L)\rangle_{r_m} = \frac{2\pi}{S}\int_0^{r_m} rdr|\theta_e(r,L)|^2, \tag{14}$$

where r_m is the cutoff radius and $S = \pi r_m^2$ the surface of collection. The measurement depends on the spatial filtering procedure (pinhole in our case) and the local echo pulse area $\theta_e(r,L)$.

3. Experimental results and discussion

3.1. Experimental setup

The crystal under investigation is 0.1 at.%Tm^{3+}:$Y_3Al_5O_{12}$ (YAG) that has been well studied as an optical quantum memory medium [53–55] due to the $^3H_6(1) \rightarrow {}^3H_4(1)$ transition at 793 nm. The inhomogeneous broadening is $\Delta_{inh} \approx 20$ GHz. The $2\times3\times8$ mm^3 crystal is cooled down to 4K in a Montana Instruments cryostat. The optical density αL along the 8 mm long dimension reaches 1.5 at the central frequency. The crystal is placed in a moderate 600 G magnetic field pointing along the [001] crystal axis. The field is provided by two pairs of 25 mm permanent NdFeB magnets (at 30 mm from the crystal). In this configuration, the optical transition coherence lifetime is increased to $T_2 = 189$ μs.

The light beams are generated by a single frequency continuous Ti:Sapphire laser. The beams pass through an acousto-optic modulator (AOM1) that temporally shapes the incoming pulses of the two-pulse photon echo sequence. We use a single mode fiber for mode filtering. Lens L1 focuses the light on the crystal with a waist $r_0 = 24.3\mu m$. Light propagates along the $[1\bar{1}0]$ crystallographic axis and is polarized along the [001] crystalline axis. The details of the mutual orientation of the crystal axes and electric and magnetic fields are shown in Fig. 1. The crystal is imaged outside the cryostat with a 75 mm lens L2, with a magnification factor $M = 4$. This results in a Gaussian beam with waist $r_p = Mr_0 = 97$ μm in the crystal image plane.

To study the effect of the spatial beam profile on the photon echo area theorem we perform two types of experiments, without spatial filtering (NoSF-experiment) and with spatial filtering (SF-experiment). With these two experiments, we evaluate how different degrees of spatial inhomogeneity affect the characteristic nutation of the detected echo pulse depending on the incoming pulse areas $\theta_1(0)$ and $\theta_2(0)$. In the NoSF-experiment, the detector is directly placed in the crystal image plane (see Fig. 4). In the SF-experiment, analogous to the works [30, 36], a 50 μm pinhole ($r_m = 25$ μm) is placed in the crystal image plane. This pinhole selects the most intense light field coming from the center of the Gaussian profile such that $E(t,r_m) = 0.93E(t,0)$. Then the lens pair L3 and L4 focuses the light transmitted by the pinhole onto AOM2 that temporally gates the echo signal and thus isolates the avalanche photodetector from the intense excitation pulses. A higher sensitivity avalanche photodetector is used for the SF experiment to compensate for the lower signal obtained after spatial filtering. Lenses L5 and L6 focus the light on the detector.

3.2. McCall-Hahn area theorem verification

We start by verifying the McCall-Hahn area theorem for a single pulse excitation. For this purpose, we carry out the experiment with spatial filtering ($r_p = 97\mu m$ and $r_m = 25\mu m$) to be as

Optics EXPRESS

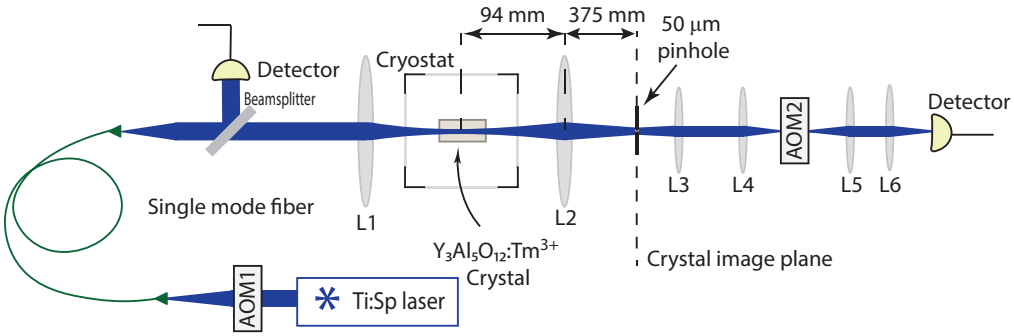

Fig. 4. Scheme of the experimental setup when spatial filtering is used (SF-experiment). Single frequency continuous Ti:Sp laser emits light at 793 nm wavelength ($^3H_4 \rightarrow ^3H_6$ transition). The 0.1 at.%Tm^{3+}:YAG crystal is placed inside the cryostat at 4K. The incoming pulses are detected before the crystal by a reference detector Thorlabs DET10A and the photon echo is detected by avalanche photodetector Thorlabs APD120A. Acousto-optic modulators AOM1 and AOM2 are driven by an arbitrary waveform generator RIGOL DG5352. The lenses L1-L6 have the following focal lengths (in mm) $f_1 = 75$, $f_2 = 75$, $f_3 = 35$, $f_4 = 200$, $f_5 = 200$ and $f_6 = 25.4$.

close as possible to the plane wave case. The pulse duration is $\delta t = 2\mu s$ and we vary the pulse amplitude to control the input area $\theta_1(0,0)$.

The obtained experimental dependence of the normalized value $A_D \sim \int dt\sqrt{U_D(t)}$ (where $U_D(t)$ is the detector signal) on the pulse area of input signal is depicted as black squares in Fig. 5. The experimental data A_D are in good agreement with theoretical curve $\langle\theta_e^2(r_m)\rangle^{1/2}$ from Eq. (14) obtained in [26].

To fit the experimental data we used two fitting parameters, the scaling coefficients for x and y axis.

3.3. Photon echo area theorem with Gaussian beams

In the NoSF-experiment, the entire beam going through the sample is collected on the detector. In this experiment no external magnetic field is applied to the crystal so the coherence lifetime $T_2 = 76\mu s$ is shorter, optical density at the line center is $\alpha L = 1.5$, with $\alpha = 187.5$ m^{-1} and $L = 8$ mm. We vary the amplitude of the second light pulse (and thus the input area $\theta_2(r,0)$), while maintaining constant the first pulse area $\theta_1(0,0)$. The pulse durations are $\delta t_1 = \delta t_2 = 2\mu s$ and the delay between the pulses is $\tau_{12} = 8\mu s$. Fig. 6 shows the experimental data for three different input areas of the first pulse: $\theta_1(0,0) \approx 0.3\pi$, 0.7π and 1.4π. The nutation behavior of the echo signal as a function of $\theta_2(0,0)$ is significantly damped for the first and second cases (see black squares and red circles in Fig. 6) and almost absent in the third case of the highest $\theta_1(0,0) \approx 1.4\pi$ (see blue triangles in Fig. 6). This is due to averaging over the transverse spatial profile of the detected echo signal as $U_D(t) \sim \int_0^\infty I_e(r,t)rdr$, since $r_m \gg r_0$ (see Eq. (14)).

Figure 6 also shows the theoretical calculations of the photon echo signal characterized by the value $\langle\theta_e^2(r_m)\rangle^{1/2}$ (see Eq. (14)) in these experimental conditions. To obtain these curves, we use only two fitting parameters, namely two scaling factors for the horizontal (absolute value of the incoming pulse area) and vertical axis (normalized value A_D). The horizontal scaling factor is proportional to the experimentally measured Rabi frequency which in this experiment was ≈ 320 kHz, which is approximately 3 times lower than in the SF-experiment.

The experimental and theoretical dependencies in Fig. 6 are in a good agreement for the small incoming pulse area $\theta_2(0,0) < 1.3\pi$ for all three curves with different values of pulse area

Optics EXPRESS

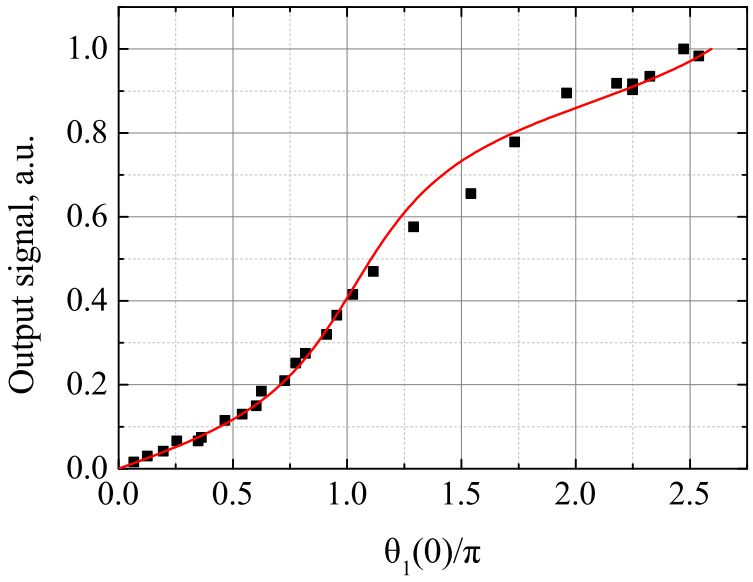

Fig. 5. Experimental (squares, normalized value $A_D \sim \int dt\sqrt{U_D(t)}$ where $U_D(t)$ is the detector signal) and theoretical (red line, $\langle\theta_e^2(r_m)\rangle^{1/2}$ from Eq. (14)) dependences of a single pulse area after the resonant medium as a function of the incoming pulse area, corresponding to the McCall-Hahn area theorem.

$\theta_1(0,0) = 0.3\pi,\ 0.7\pi,\ 1.4\pi$. As expected, the experimental behavior of echo signal deviates from the theoretical solution Eq. (14) at higher pulse area $\theta_2(0,0)$. One reason for this is that the experimentally detected pulse intensities cannot be expressed in terms of pulse areas for $\theta_1(0), \theta_2(0) > \pi$ due to the transverse oscillating spatial behavior. Moreover, we observe an increased optical nutation period at higher input pulse area $\theta_2(0,0)$ as compared to the theoretical curves. This non-obvious nonlinear effect of multi-pulse excitation deserves a special study and is beyond the scope of this paper. Perspectives are discussed in the conclusion.

3.4. Photon echo area theorem with spatially filtered beams

To retrieve the echo nutation, we perform the SF-experiment using a pinhole for the detection as depicted in Fig. 4 with estimated Gaussian beam radius $r_p = 97\mu m$ at the pinhole location. We realize two sets of measurements by collecting the echo signal for varying incoming pulse areas $\theta_1(0,0)$ and $\theta_2(0,0)$. In this section, the experimental parameters are $r_p = 97\mu$m, $r_m = 25\mu$m, $L = 8$mm, $\alpha = 187.5\text{m}^{-1}$, $T_2 = 189\mu$s, the measured Rabi frequency of the transition $\Omega \approx 900$ kHz. They are also used for the numerical calculations from Eqs. (6) and (14). The pulse durations are $\delta t_1 = 5\mu s,\ \delta t_2 = 2\ \mu s$ and the time delay between the exciting pulses is $\tau_{12} = 20\mu$s.

Figure 7 shows the experimental and theoretical echo signal dependencies as a function of the second pulse area for two different values of the first pulse input area. Again, we also use two fitting parameters (scaling factors for both axis). The horizontal scaling factor is the same as for single pulse dependence in Fig. 5. Each pair (experimental data set and theoretical curve) corresponds to a given value of the first pulse incoming area $\theta_1(0,0)$. Figure 7 shows that spatial filtering reveals the nutation and significantly reduces the damping. The particular case of $\theta_1(0,0) < 1$ was experimentally studied earlier in [30] for $\theta_2(0,0) < 2\pi$ where the obtained results were satisfactorily described by the plane wave solution (Eq. (9)).

We note that both theoretical curves and experimental data, exhibit a series of damped

Optics EXPRESS

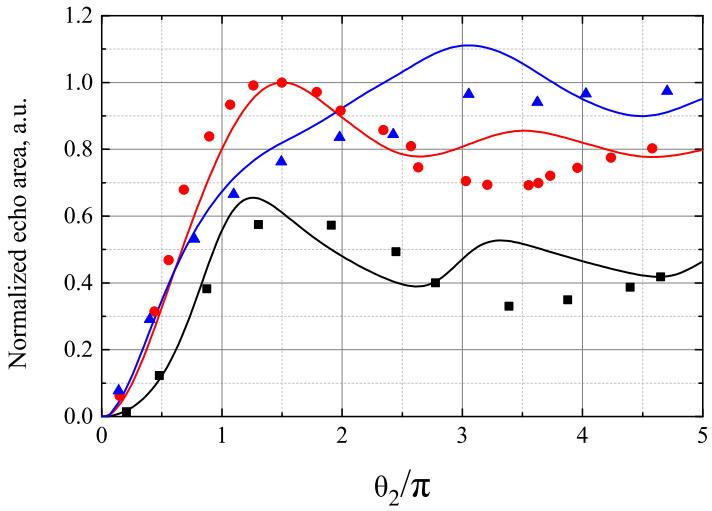

Fig. 6. Three experimental (symbols, normalized value $A_D \sim \int dt\sqrt{U_D(t)}$ where $U_D(t)$ is the detector signal) and the corresponding theoretical (lines, normalized value $\sim \langle\theta_e^2(r_m)\rangle^{1/2}$ from Eq. (14)) dependencies of the photon echo pulse signal as a function of the incoming area of the second pulse. Each set corresponds to a different initial area of the first incoming pulse. Black squares and black line correspond to $\theta_1(r = 0, z = 0) = \theta_1(0, 0) \approx 0.3\pi$, red circles and red line to $\theta_1(0, 0) \approx 0.7\pi$, blue triangles and blue line to $\theta_1(0, 0) \approx 1.4\pi$.

oscillations. The agreement is quite accurate at low input pulse area $\theta_2(0, 0) < 2\pi$. However, at higher $\theta_2(0, 0)$, the experimental curves are strongly damped as compared to the theoretical prediction. The curves are stretched in the large area region showing a clear non-harmonic behavior. The increase of the nutation period is an interesting feature that we see much more clearly than in the NoSF-experiment. This general discrepancy indicates the limitations of the geometrical optics approximation that we assumed in averaging over the beam profile. This issue will be also discussed in the conclusion.

We also study the experimental echo signal (black squares in Fig. 8) as a function of the first pulse area $\theta_1(0, 0)$. The solid line is the theoretical fit (see Fig. 8) following a similar procedure to Fig. 7. As before, we plot the theoretical value $\langle\theta_e^2(r_m)\rangle^{1/2}$ (from Eq. (14)) and the experimental data as $\int dt\sqrt{U_D}$ for constant $\theta_2(0, 0) = 1.1\pi$. Again, the theory coincides with the observed data at small input pulse area $\theta_1(0, 0) < \pi$ and only qualitatively describes the nutation at higher $\theta_1(0, 0)$ values where the observed oscillations are strongly damped.

Both dependencies of echo signal on $\theta_2(0, 0)$ and $\theta_1(0, 0)$ demonstrate quite similar features for increasing $\theta_2(0, 0)$ and $\theta_1(0, 0)$. Namely, we observe the oscillation stretching of the experimental curve (longer periods at higher areas). The similar pattern indicates common physical effects in the observed nutation taking place in an optically dense medium.

4. Discussion and conclusion

We have performed theoretical and experimental studies of two-pulse photon echo in the optically dense medium. We have used the optical transition $^3H_6(1) \rightarrow {}^3H_4(1)$ (793 nm) of a Tm ion-doped YAG crystal cooled at 4K. Herein, the echo area has been studied as a function of incoming pulse areas of the first $\theta_1(0, 0)$ and second $\theta_2(0, 0)$ pulses up to 4π and 7π, respectively. We have observed that inhomogeneous beam intensity profile leads to the strong damping of the expected

Optics EXPRESS

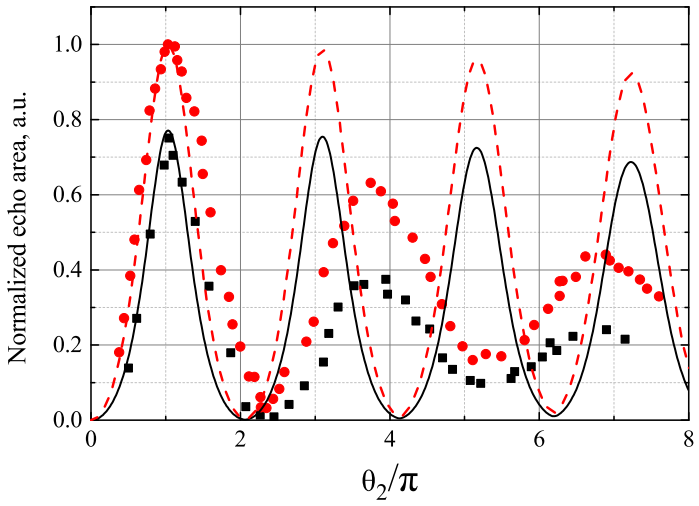

Fig. 7. Experimental (symbols, normalized value $A_D \sim \int \sqrt{U_D} dt$) and theoretical (lines, normalized value $\sim \langle \theta_e^2(r_m) \rangle^{1/2}$ from Eq. (14) with $r_0 = 97\mu$m, $r_m = 25\mu$m) dependencies of the primary photon echo signal on the incoming area of the second pulse. Black squares and black solid line correspond to $\theta_1(0,0) = 0.25\pi$, red circles and red dashed line correspond to $\theta_1(0,0) = 0.4\pi$. See text for details.

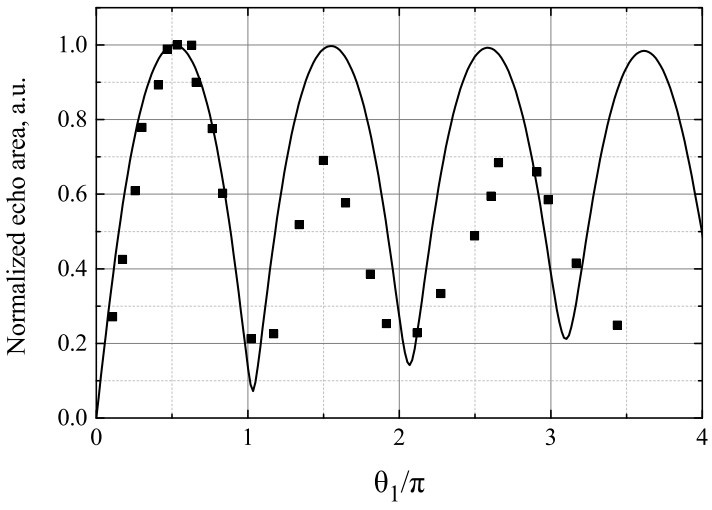

Fig. 8. Experimental (squares, normalized $A_D \sim \int \sqrt{U_D} dt$) and theoretical ($\langle \theta_e^2(r_m) \rangle^{1/2}$ from Eq. (14) with $r_0 = 97\mu$m, $r_m = 25\mu$m) dependencies of primary photon echo signal on the first incoming pulse area $\theta_1(0,0)$ with constant $\theta_2(0,0) = 1.1\pi$. See text for details.

Optics EXPRESS

nutation. Subsequent experiments with spatial filtering allowed us to retrieve the nutation.

To analyze the experimental data we have developed a theoretical approach based on the photon echo area theorem. We applied the theorem for two-dimensional Maxwell-Bloch model with spatial transverse inhomogeneity of the light beams considered in the geometrical optics approximation. This model satisfyingly describes the data for relatively small incoming pulse areas $\theta_1(0,0), \theta_2(0,0) < 2\pi$ and provides a qualitative agreement of the observed echo signal nutation at higher input pulse areas. In this region the theorem also predicts the energy efficiency of the echo in agreement with Maxwell-Bloch simulations presented in [36].

We also note that the geometrical optics approximation cannot describe the self-focusing and de-focusing of the beams propagating in an optically dense and spectrally selective atomic medium. Including the non-linear diffraction in the paraxial Helmholtz equation is a complex analytical task which is beyond the scope of this work. Atomic dipole-dipole interactions, as instantaneous spectral diffusion [56–58], cannot be also completely discarded.

Finally, the photon echo pulse area theorem provides a useful and general tool to study the light-atom interactions [59–62] revealing fundamental processes that play a role in many quantum optical memory protocols realized in the optically dense media [19, 63–66].

Appendix

The photon echo area theorem was obtained in [44]. Here we present a derivation of the theorem in terms of Bloch vector variables (u, v, w), complex light field envelope $E(t,z) = \varepsilon(t,z)\exp[i(kz-\omega t)] + c.c.$ and Rabi frequency $\Omega(t,z) = (2d/\hbar)\varepsilon(t,z)$. We start from the usual reduced set of Maxwell-Bloch equations [42] for the light field and atomic polarization:

$$\left(\frac{\partial}{\partial z} + \frac{\partial}{c\,\partial t}\right)\Omega(t,z) = i\frac{\mu}{2}\langle P_{12}(t,z,\Delta)\rangle, \tag{15}$$

$$\frac{\partial}{\partial t}u(t,z,\Delta) = -\Delta v(t,z,\Delta) - \gamma u(t,z,\Delta), \tag{16}$$

$$\frac{\partial}{\partial t}v(t,z,\Delta) = \Delta u(t,z,\Delta) - \gamma v(t,z,\Delta) - \Omega(t,z)w(t,z,\Delta), \tag{17}$$

$$\frac{\partial}{\partial t}w(t,z,\Delta) = \Omega(t,z)v(t,z,\Delta), \tag{18}$$

where $\mu = 4\pi N d^2\omega/\hbar c$ and $\langle ...\rangle \equiv \int_{-\infty}^{\infty} G(\Delta)...d\Delta$ is the averaging over the inhomogeneous broadening.

The formal solution of Eqs. (16) and (17) can be written as:

$$P_{12}(t,z,\Delta) = [u(t,z,\Delta) - iv(t,z,\Delta)] = P_{12}(t_0,z,\Delta)e^{-(i\Delta+\gamma)(t-t_0)} - i\int_{t_0}^{t} dt'\Omega(t',z)w(t',z,\Delta)e^{-(i\Delta+\gamma)(t-t')}. \tag{19}$$

Substituting the solution for $P_{12}(t,z,\Delta)$ in Eq. (15) and integrating it over the time period of the specific pulse $[t_0, t_0+\tau_{12}]$, (where $t_0 = t_e - \tau_{12}/2$, t_e is the time of the echo emission, τ_{12} is the time delay between the pulses) we get:

$$\frac{\partial}{\partial z}\theta(z) = i\frac{\mu}{2}\left[\int_{t_0}^{t_0+\tau_{12}} dt\langle P_{12}(t_0,z,\Delta)e^{-(i\Delta+\gamma)(t-t_0)}\rangle - i\int_{t_0}^{t_0+\tau_{12}} dt\int_{t_0}^{t} dt'\Omega(t',z)\langle w(t',z,\Delta)e^{-(i\Delta+\gamma)(t-t')}\rangle \right. \tag{20}$$

Optics EXPRESS

We are especially interested in the formation of a primary photon echo with emission time $t_e = 2\tau_{12}$ in the limit of a sufficiently large time delay between the two incoming light pulses $\tau_{12} \gg \delta t_i$ (where δt_i is a temporal duration of the i-th input light pulses).

After the action of the two light pulses, the atomic variables P_{12} and w acquire several components characterized by different spectral properties. Two components of the coherence P_{12} describe the dephasing of the atomic coherence $P_1 e^{-i(\Delta - i\gamma)t}$ and $P_2 e^{-i(\Delta - i\gamma)(t-\tau_{12})}$ (the free induction decay terms after the first and the second pulses) and the only component characterizing the coherence rephasing determining the emission of the primary echo $P_3 e^{-i\Delta(t-2\tau_{12})} e^{-\gamma t}$ at time $t = 2\tau_{12}$. In the limit of $\Delta \to 0$, these atomic coherences take the forms: $P_1 \to -i \sin\theta_1(z) \cos^2\theta_2(z)/2$, $P_2 \to -i \cos\theta_1(z) \sin\theta_2(z)$ and $P_3 \to (-i) v_e(t_0, z, 0) = -i \sin\theta_1(z) \sin^2\theta_2(z)/2$ [3, 42]. The echo field is irradiated initially by the rephasing polarization P_3 and highly modified during propagation by the acquired atomic inversion w.

Herein, after the two pulses exit the medium, the atomic inversion w contains two components $w = w_1 + w_2$ characterized by different spectral properties. In the limit of $\Delta \to 0$, we have $w_1 \to w_0 \cos\theta_1(z) \cos\theta_2(z)$ and $w_2 \to -w_0 \sin\theta_1(z) \sin\theta_2(z) e^{-\gamma\tau_{12}} \cos\Delta\tau_{12}$ as studied in [67]. Here we assume that the input light pulses are well separated with the time delay between pulses being much larger than the temporal duration of the light pulses. With the averaging over inhomogeneous broadening of atomic transition $\langle ... \rangle$ in Eq. (15), only those components of polarization P_{12} and w will participate in the echo formation due to their rephasing at the time of the echo emission. Namely the terms P_3 and w_1 affect the echo field emission while the other terms disappear after the averaging over the inhomogeneous broadening in the limit $\tau_{12} \gg \delta t_e$ (where δt_e is a temporal duration of the echo pulse $\delta t_e \sim \delta t$). Taking into account these properties of different spectral components in the averaged polarization and inversion, we can write for the averaged atomic coherence

$$\langle P_{12}(t_0, z, \Delta) e^{-(i\Delta+\gamma)(t-t_0)} \rangle \,|_{echo} \cong e^{-2\gamma\tau_{12}} \langle P_3(t_0, z, \Delta) e^{-i\Delta(t-2\tau_{12})} \rangle, \tag{21}$$

$$\langle w(t_0, z, \Delta) \rangle \cong \langle w_1(t_0, z, \Delta) \rangle. \tag{22}$$

Funding

Russian Science Foundation (RSF) (14-12-01333-P); Investissements d'Avenir du LabEx PALM ExciMol and OptoRF-Er (ANR-10-LABX-0039-PALM); ITMO Cancer AVIESAN (National Alliance for Life Sciences & Health).

References

1. E. L. Hahn, "Spin echoes," Phys. Rev. **80**, 580–594 (1950).
2. U. K. Kopvillem and V. R. Nagibarov, "Luminous echo of paramagnetic crystals," Fiz. Met. i Met. **15**, 313–315 (1963).
3. N. A. Kurnit, I. D. Abella, and S. R. Hartmann, "Observation of a photon echo," Phys. Rev. Lett. **13**, 567–568 (1964).
4. E. A. Rotberg, B. Barrett, S. Beattie, S. Chudasama, M. Weel, I. Chan, and A. Kumarakrishnan, "Measurement of excited-state lifetime using two-pulse photon echoes in rubidium vapor," J. Opt. Soc. Am. B **24**, 671–680 (2007).
5. K. E. Dorfman, F. Schlawin, and S. Mukamel, "Nonlinear optical signals and spectroscopy with quantum light," Rev. Mod. Phys. **88**, 045008 (2016).
6. M. S. Pshenichnikov, K. Duppen, and D. A. Wiersma, "Time-resolved femtosecond photon echo probes bimodal solvent dynamics," Phys. Rev. Lett. **74**, 674–677 (1995).
7. N. Morita and T. Yajima, "Ultrahigh-time-resolution coherent transient spectroscopy with incoherent light," Phys. Rev. A **30**, 2525–2536 (1984).
8. P. C. Becker, H. L. Fragnito, J. Y. Bigot, C. H. Brito Cruz, R. L. Fork, and C. V. Shank, "Femtosecond photon echoes from molecules in solution," Phys. Rev. Lett. **63**, 505–507 (1989).
9. E. T. J. Nibbering, D. A. Wiersma, and K. Duppen, "Femtosecond non-markovian optical dynamics in solution," Phys. Rev. Lett. **66**, 2464–2467 (1991).
10. S. V. Konturov, V. S. Lobkov, K. M. Salikhov, V. V. Samartsev, G. M. Safiullin, and V. A. Zuikov, "Femtosecond photon echo in dye-doped polymer film at liquid nitrogen temperature," Laser Phys. Lett. **2**, 21–24 (2005).
11. E. I. Shtyrkov and V. V. Samartsev, "Imaging properties of dynamic echo-holograms in resonant media," Optika i Spektroskopiia **40**, 392–393 (1976).

Optics EXPRESS

12. C. V. Heer and P. F. McManamon, "Wavefront correction with photon echoes," Opt. Commun. **23**, 49 – 50 (1977).
13. N. S. Shiren, "Generation of time-reversed optical wave fronts by backward-wave photon echoes," Appl. Phys. Lett. **33**, 299–300 (1978).
14. E. I. Shtyrkov, V. S. Lobkov, S. A. Moiseev, and N. G. Yarmukhametov, "Characteristics of reversed photon echo resulting from nonsimultaneous four-wave interaction in ruby," Zh. Eksp. Teor. Fiz. **81**, 1041–1046 (1981).
15. T. W. Mossberg, "Time-domain frequency-selective optical data storage," Opt. Lett. **7**, 77–79 (1982).
16. N. W. Carlson, L. J. Rothberg, A. G. Yodh, W. R. Babbitt, and T. W. Mossberg, "Storage and time reversal of light pulses using photon echoes," Opt. Lett. **8**, 483–485 (1983).
17. S. A. Moiseev and S. Kröll, "Complete reconstruction of the quantum state of a single-photon wave packet absorbed by a doppler-broadened transition," Phys. Rev. Lett. **87**, 173601 (2001).
18. M. P. Hedges, J. J. Longdell, Y. Li, and M. J. Sellars, "Efficient quantum memory for light," Nature **465**, 1052–1056 (2010).
19. W. Tittel, M. Afzelius, T. Chanelière, R. Cone, S. Kröll, S. Moiseev, and M. Sellars, "Photon-echo quantum memory in solid state systems," Laser & Photonics Rev. **4**, 244–267 (2009).
20. M. Hosseini, B. Sparkes, G. Campbell, P. Lam, and B. Buchler, "High efficiency coherent optical memory with warm rubidium vapour," Nat. Commun. **2** (2011).
21. M. Hosseini, G. Campbell, B. M. Sparkes, P. K. Lam, and B. C. Buchler, "Unconditional room-temperature quantum memory," Nat. Phys. **7**, 794 (2011).
22. M. Sabooni, Q. Li, S. Kröll, and L. Rippe, "Efficient quantum memory using a weakly absorbing sample," Phys. Rev. Lett. **110**, 133604 (2013).
23. V. Damon, M. Bonarota, A. Louchet-Chauvet, T. Chanelière, and J.-L. L. Gouët, "Revival of silenced echo and quantum memory for light," New J. Phys. **13**, 093031 (2011).
24. Y. Rostovtsev, Z. Sariyianni, and M. Scully, "Photon echo pulse shape storage," Laser physics **12**, 1148–1154 (2002).
25. J. Ruggiero, J.-L. Le Gouët, C. Simon, and T. Chanelière, "Why the two-pulse photon echo is not a good quantum memory protocol," Phys. Rev. A **79**, 053851 (2009).
26. S. L. McCall and E. L. Hahn, "Self-induced transparency," Phys. Rev. **183**, 457–485 (1969).
27. J. Eberly, "Area theorem rederived," Opt. Express **2**, 173–176 (1998).
28. J. H. Eberly and V. V. Kozlov, "Wave equation for dark coherence in three-level media," Phys. Rev. Lett. **88**, 243604 (2002).
29. J.-C. Delagnes and M. Bouchene, "Beyond the pulse-area theorem: Role of the absorption and the dispersion in the propagation of weak ultrashort resonant pulses," Opt. Commun. **281**, 5824–5829 (2008).
30. J. Ruggiero, T. Chanelière, and J.-L. Le Gouët, "Coherent response to optical excitation in a strongly absorbing rare-earth ion-doped crystal," J. Opt. Soc. Am. B **27**, 32–37 (2010).
31. X.-y. Yu, W. Liu, and C. Li, "Near-resonant propagation of short pulses in a two-level medium," Phys. Rev. A **84**, 033811 (2011).
32. T. Chanelière, "Strong excitation of emitters in an impedance matched cavity: the area theorem, π-pulse and self-induced transparency," Opt. Express **22**, 4423–4436 (2014).
33. G. Shchedrin, C. O'Brien, Y. Rostovtsev, and M. O. Scully, "Analytic solution and pulse area theorem for three-level atoms," Phys. Rev. A **92**, 063815 (2015).
34. R. Gutiérrez-Cuevas and J. H. Eberly, "Vector-soliton storage and three-pulse-area theorem," Phys. Rev. A **94**, 013820 (2016).
35. T. Wang, C. Greiner, and T. Mossberg, "Photon echo signals: beyond unit efficiency," Opt. Commun. **153**, 309–313 (1998).
36. T. Wang, C. Greiner, J. R. Bochinski, and T. W. Mossberg, "Experimental study of photon-echo size in optically thick media," Phys. Rev. A **60**, R757–R760 (1999).
37. T. Chang, M. Tian, and W. Randall Babbitt, "Numerical modeling of optical coherent transient processes with complex configurations - I. Angled beam geometry," J. Lumin. **107**, 129–137 (2004).
38. T. Chang, M. Tian, Z. W. Barber, and W. Randall Babbitt, "Numerical modeling of optical coherent transient processes with complex configurations-II. Angled beams with arbitrary phase modulations," J. Lumin. **107**, 138–145 (2004).
39. T. Chang and M. Tian, "Numerical modeling of optical coherent transient processes with complex configurations-III: Noisy laser source," J. Lumin. **127**, 76–82 (2007).
40. E. L. Hahn, N. S. Shiren, and S. L. McCall, "Application of the area theorem to phonon echoes," Phys. Lett. A **37**, 265 – 267 (1971).
41. R. Friedberg and S. Hartmann, "Superradiant damping and absorption," Phys. Lett. A **37**, 285 – 286 (1971).
42. L. Allen and J. Eberly, *Optical Resonance and Two-level Atoms*, Dover books on physics and chemistry (Dover, 1975).
43. M. Azadeh, C. Sjaarda Cornish, W. R. Babbitt, and L. Tsang, "Efficient photon echoes in optically thick media," Phys. Rev. A **57**, 4662–4668 (1998).
44. S. A. Moiseev, "Some general nonlinear properties of photon-echo radiation in optically dense media," Opt. Spectrosc. (English translation Optika i Spektroskopiya) **62**, 180–185 (1987).
45. S. A. Moiseev, "Quantum memory for intense light fields in the photon echo technique," Izv. Ross. Akad. Nauk, Ser. Fiz. **68**, 1260–1264 (2004).
46. A. M. Dibos, M. Raha, C. M. Phenicie, and J. D. Thompson, "Atomic source of single photons in the telecom band,"

Optics EXPRESS

Phys. Rev. Lett. **120**, 243601 (2018).
47. B. Casabone, J. Benedikter, T. Hümmer, F. Oehl, K. de Oliveira Lima, T. W. Hänsch, A. Ferrier, P. Goldner, H. de Riedmatten, and D. Hunger, "Cavity-enhanced spectroscopy of a few-ion ensemble in Eu^{3+}:Y_2O_3," New J. Phys. **20**, 095006 (2018).
48. T. Zhong, J. M. Kindem, J. G. Bartholomew, J. Rochman, I. Craiciu, V. Verma, S. W. Nam, F. Marsili, M. D. Shaw, D. Beyer, and A. Faraon, "Optically addressing single rare-earth ions in a nanophotonic cavity," Phys. Rev. Lett. **121**, 183603 (2018).
49. G. L. Lamb, "Analytical descriptions of ultrashort optical pulse propagation in a resonant medium," Rev. Mod. Phys. **43**, 99–124 (1971).
50. T. Chanelière, G. Hétet, and N. Sangouard, "Chapter two - quantum optical memory protocols in atomic ensembles," (Academic Press, 2018), pp. 77 – 150.
51. C. S. Cornish, W. Babbitt, and L. Tsang, "Demonstration of highly efficient photon echoes," Opt. Letters **25**, 1276–1278 (2000).
52. A. E. Siegman, "Unstable optical resonators for laser applications," Proc. IEEE **53**, 277–287 (1965).
53. T. Chanelière, M. Bonarota, V. Damon, R. Lauro, J. Ruggiero, I. Lorgeré, and J.-L. L. Gouët, "Light storage protocols in Tm:YAG," J. Lumin. **130**, 1572–1578 (2010).
54. M. Bonarota, J.-L. L. Gouët, and T. Chanelière, "Highly multimode storage in a crystal," New J. Phys. **13**, 013013 (2011).
55. K. Gerasimov, M. Minnegaliev, S. Moiseev, R. Urmancheev, T. Chanelière, and A. Louchet-Chauvet, "Quantum memory in an orthogonal geometry of silenced echo retrieval," Opt. Spectrosc. (English translation Optika i Spektroskopiya) **123**, 211–216 (2017).
56. J. Huang, J. M. Zhang, A. Lezama, and T. W. Mossberg, "Excess dephasing in photon-echo experiments arising from excitation-induced electronic level shifts," Phys. Rev. Lett. **63**, 78–81 (1989).
57. G. K. Liu and R. L. Cone, "Laser-induced instantaneous spectral diffusion in Tb^{3+} compounds as observed in photon-echo experiments," Phys. Rev. B **41**, 6193–6200 (1990).
58. C. W. Thiel, R. M. Macfarlane, Y. Sun, T. Böttger, N. Sinclair, W. Tittel, and R. L. Cone, "Measuring and analyzing excitation-induced decoherence in rare-earth-doped optical materials," Laser Phys. **24**, 106002 (2014).
59. M. Fleischhauer and S. F. Yelin, "Radiative atom-atom interactions in optically dense media: Quantum corrections to the lorentz-lorenz formula," Phys. Rev. A **59**, 2427–2441 (1999).
60. L. Corman, J. L. Ville, R. Saint-Jalm, M. Aidelsburger, T. Bienaimé, S. Nascimbène, J. Dalibard, and J. Beugnon, "Transmission of near-resonant light through a dense slab of cold atoms," Phys. Rev. A **96**, 053629 (2017).
61. A. M. Basharov, "Stark interaction of identical particles with the vacuum electromagnetic field as quantum poisson process suppressing collective spontaneous emission," Phys. Rev. A **84**, 013801 (2011).
62. A. M. Basharov, ""Trapping" of the radiation of an excited particle by its stark interaction with the nonresonant levels of surrounding particles," JETP Lett. **107**, 143–150 (2018).
63. A. I. Lvovsky, B. C. Sanders, and W. Tittel, "Optical quantum memory," Nat. Photonics **3**, 706–714 (2009).
64. K. Hammerer, A. S. Sørensen, and E. S. Polzik, "Quantum interface between light and atomic ensembles," Rev. Mod. Phys. **82**, 1041–1093 (2010).
65. C. Simon, M. Afzelius, J. Appel, A. Boyer De La Giroday, S. J. Dewhurst, N. Gisin, C. Y. Hu, F. Jelezko, S. Kröll, J. H. Müller, J. Nunn, E. S. Polzik, J. G. Rarity, H. De Riedmatten, W. Rosenfeld, A. J. Shields, N. Sköld, R. M. Stevenson, R. Thew, I. A. Walmsley, M. C. Weber, H. Weinfurter, J. Wrachtrup, and R. J. Young, "Quantum memories," Eur. Phys. J. D **58**, 1–22 (2010).
66. K. Heshami, D. G. England, P. C. Humphreys, P. J. Bustard, V. M. Acosta, J. Nunn, and B. J. Sussman, "Quantum memories: emerging applications and recent advances," J. Mod. Opt. **63**, 2005–2028 (2016).
67. N. F. Ramsey, "A molecular beam resonance method with separated oscillating fields," Phys. Rev. **78**, 695–699 (1950).